J Mater Sci: Mater Electron (2017) 28:5021–5028
DOI 10.1007/s10854-016-6158-x

Thickness dependence of properties Ga-doped ZnO thin films deposited by magnetron sputtering

H. Mahdhi[1] · J. L. Gauffier[2] · K. Djessas[3] · Z. Ben Ayadi[1]

Received: 5 September 2016 / Accepted: 29 November 2016 / Published online: 9 December 2016
© Springer Science+Business Media New York 2016

Abstract In this work, we studied gallium doped zinc oxide (ZnO:Ga) thin films deposited by rf-magnetron sputtering at room temperature using gallium doped nanocrystalline powder synthesized by sol–gel method. The effect of the thickness, on the physical properties of the GZO thin films was analyzed. The influence of the thickness, on structure, surface morphologies, chemical atomic composition, electrical and optical properties was investigated by XRD, SEM, TEM, AFM, Hall measurement and UV Vis–NIR spectrophotometer, respectively. X-ray diffraction (XRD) results revealed the polycrystalline nature of the films with hexagonal wurtzite structure having preferential orientation along [002] direction normal to the substrate. The lowest resistivity obtained from electrical studies was 10^{-4} Ω cm. Optical transmittance measurement results show a good transparency within the visible wavelength range for all the films.

1 Introduction

Transparent conductive oxide films (TCOs) have been extensively investigated due to their broad range of applications such as transparent electrodes in solar cells and in photovoltaic devices [1–3]. Zinc oxide (ZnO) has recently attracted much attention as a promising alternative material because of its low cost and its relatively low deposition temperature, besides its optical and electrical properties comparable to those of indium tin oxide (ITO). These advantages are of considerable interest for practical applications such as transparent electrodes, window material in displays, solar cells, and various optoelectronic devices [4, 5]. Several techniques of deposition have been used for the production of ZnO thin films, such as thermal evaporation [6], chemical vapor deposition [7], RF magnetron sputtering [8], spray pyrolysis [9], pulsed laser deposition [10, 11] and sol–gel process [12, 13]. However, among these techniques, sputtering and sol–gel processes offered much more advantages. Sputtering performs high deposition rate, with no toxic gas emissions, is easy to expand to large scale glass substrates with no undesired layer formation problems [14], and is low cost and simple method. On the other hand, sol–gel technique emerged within the last two decades and quickly became one of the most important and promising new material fabrication methods. On the other hand, the sol–gel technique emerged within the last two decades and quickly became one of the most important and promising new material fabrication methods. Indeed, besides the fact that it is a low cost technique, it enables researchers to easily design and fabricate a wide variety of different materials, including the possibility of doping even at high level concentrations at room temperature. Compared with other techniques, the sol–gel method has many advantages such as low cost, simple synthesis equipment, easy fabrication of large areas, easier adjustment of composition, and being able to carry out doping at molecular level. It is especially suitable for the fabrication of oxide nanoparticles [15].

Magnetron sputtering has been used by most researchers to grow ZnO thin films alloyed by Mg, Al, Ca, In, V and

✉ H. Mahdhi
hayetmahdhi@yahoo.fr

1 Laboratory of Physics of Materials and Nanomaterials applied at Environment (LaPhyMNE), Faculty of Sciences, Gabes University, Gabes, Tunisia

2 Département de Physique, INSA de Toulouse, 135 Avenue de Rangueil, 31077 Toulouse Cedex 4, France

3 Laboratoire Procédés, Matériaux et Energie Solaire (PROMES-CNRS), TECNOSUD, Rambla de la thermodynamique, 66100 Perpignan, France

Co in order to tailor the band gaps. In our previous works, the influence of Ga-doping on the structure and optical properties of ZnO films was investigated [16].

In this paper, high-quality GZO transparent conductive films are prepared by rf-magnetron sputtering from aerogel nanopowders, and their structural, electrical and optical properties are investigated as a function of their preparation conditions.

2 Experimental details

Nanocrystalline ZnO:Ga aerogels were in the first step prepared by the sol–gel method using 16 g of zinc acetate dehydrate [$Zn(CH_3COO)$, $2H_2O$] as a precursor in 112 ml of methanol. After 30 min under magnetic stirring at room temperature, an adequate quantity of calcium chloride-6-hydrate [GaN_3O_9] corresponding to [Ga/Zn] ratios of 0.00 and 0.03 was added. After 15 min under magnetic stirring, the solution was placed in an autoclave and dried in a supercritical condition of ethanol (EtOH). Then, the ZnO:Ga films were deposited on glass substrate by a conventional rf magnetron sputtering system with 10−5 mbar base pressure. A power supply operated at a crystal-controlled frequency of 13.56 MHz. After introducing the sputtering Argon gas with 99.9999% high purity without oxygen, the sputtering deposition was carried out at pressure of 10−3 mbar. The sputtering targets were prepared from the aerogel powders of GZO. During the sputtering process, the substrate temperature was set at room temperature, the RF power was 60 W and the thickness was between 200 and 1000 nm. Before deposition of the GZO thin films, the substrate glasses with 1 mm thickness were ultrasonically cleaned in HCl, rinsed in deionized water, then subsequently in ethanol and rinsed again. Other details on the experimental procedure used to elaborate our samples were reported in previous studies [15–18].

The structural, morphological, electrical, and optical properties were studied in this work. The crystal structure was characterized by X-ray diffraction (XRD) using CoKa radiation (1.78091 Å). The crystallite size was calculated from XRD data using Scherrer's formula. The GZO nanoparticles were also characterized by transmission electron microscopy (TEM) using JEM-200CX. The composition studies were performed by Energy Dispersive X-ray Spectroscopy (EDS) using a scanning electron microscope JEOL JSM 5410 type with a probe. Surface morphology and roughness were measured using atomic force microscopy (AFM, Topo Metrix) and scanning electron microscopy (SEM, HITACHI S4500). The optical transmittance measurements were performed with a Shimadzu UV-3101 PC spectrophotometer in the wavelength range from 200 to 3000 nm.

3 Results and discussion

3.1 Structural and morphological of the aerogel nanopowder

The XRD patterns of ZnO and ZnO:Ga3% are shown in Fig. 1. Three pronounced ZnO diffraction peaks appear at $2\theta = 36.66°$, $39.98°$ and $42.03°$, corresponding to (100), (002) and (101) planes respectively, which are very close to wurtzite ZnO ones [19]. The obtained XRD diffractogram matched well with the space group P63mc (No. 36–1451) of wurtzite ZnO structure [15, 19]. This result indicates that ZnO:Ga aerogel powder has a polycrystalline hexagonal wurtzite structure. Diffraction lines of ZnO were broad, and diffraction broadening was found to be dependent on Miller indices of the corresponding sets of crystal planes. The average grain size was calculated using Scherrer's formula [20]:

$$G = \frac{0.9\lambda}{\beta \cos \theta} \tag{1}$$

where λ is the X-ray wavelength (1.78901 Å), θ is the maximum of the Bragg diffraction peak (in radians) and β is the full width at half maximum (FWHM) of the XRD peak. The average grain size of the basal diameter of the cylinder-shape crystallites varies from 14 to 20 nm, whereas the height of the crystallites varies from 25 to 34 nm.

TEM measurements (Fig. 2a) show that very small particles of ZnO:Ga are present in this powder as prepared in the sol–gel. The majority of ZnO particles size present in this powder has a size between 20 and 30 nm, in a good agreement with particles size deduced from XRD spectra.

The EDX analysis shown in is shown in Fig. 2b and Table 1 confirmed the presence of gallium in the matrix

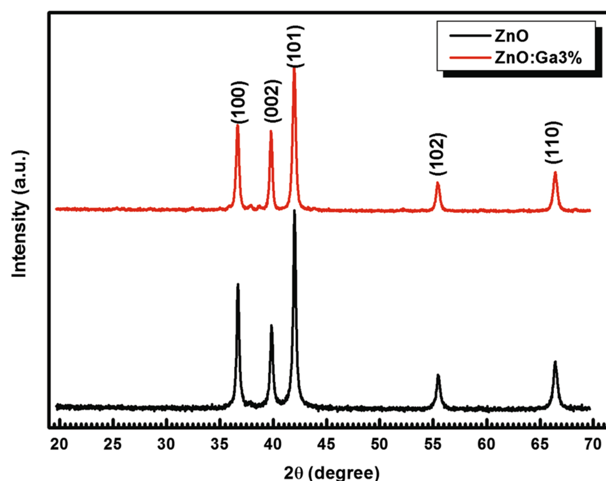

Fig. 1 X-ray diffraction of Ga-doped ZnO aerogel nanoparticles

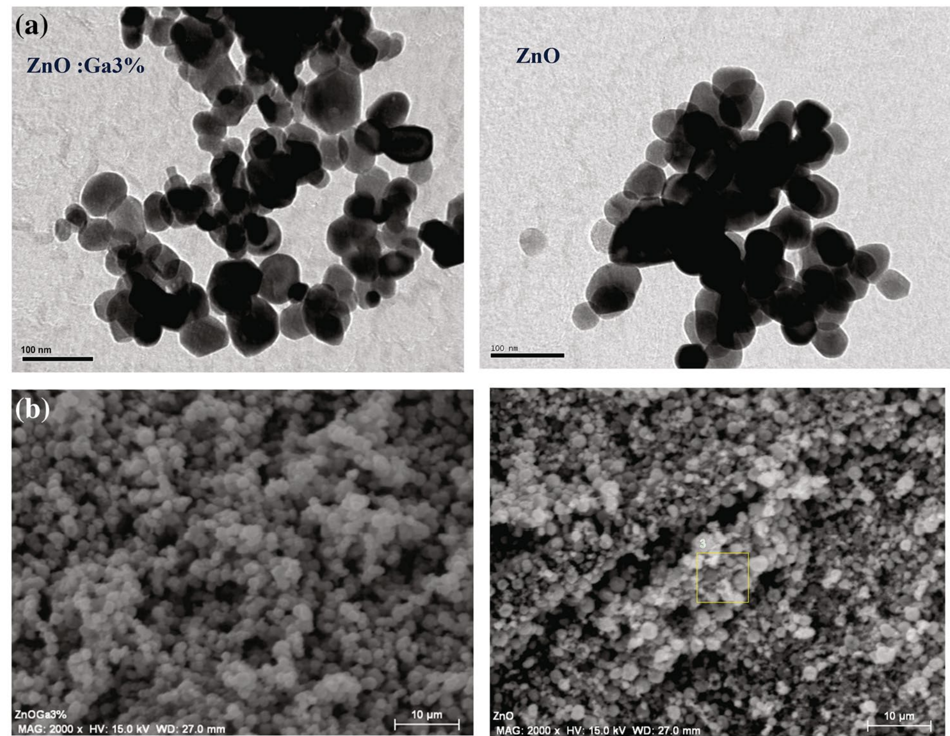

Fig. 2 TEM (**a**) and SEM (**b**) micrographs showing the general morphology of GZO aerogel nanoparticles

Table 1 Atomic compositions of ZnO and ZnO:Ga nanoparticles

Chemical composition in at.%		
Zn	O	Ga
48.43	51.57	0.00
47.12	51.54	1.34

of ZnO and absence of other impurities. From these analyses, we can conclude that the GZO nanoparticles are homogeneous and quasi-stoichiometric. A similar behaviorwas observed by Mahdhi et al. [16] and Medjnoun et al. [21].

3.2 Structural properties of GZO films

The X-ray diffraction spectra of ZnO:Ga thin films deposited at room temperature with different thickness, and films deposited from a fixed concentration, [Ga/Zn] = 3at.% are shown in Fig. 3. All films have hexagonal wurtzite structure. A prominent (002) peak indicates that the crystallite structure of the films is oriented with their c-axis perpendicular to the substrate plane [22]. The films are developed without any second phase, indicating that they have a high quality crystalline structure. Indeed, it has been established that the preferred orientation is a result of a self-ordering caused by the minimization of the crystal surface energy [23]. It is clear that the crystallinity of the ZnO:Ga layers is improved with the increase in thickness as indicated by the increase in the peak intensity (002) (Table 2). In addition, there is the filtering of this peak and its shift towards larger angles that is to say towards the position of one of ZnO powder, namely 2θ = 40°. These results indicate that the quality of the thin film is improved with the thickness (Table 3).

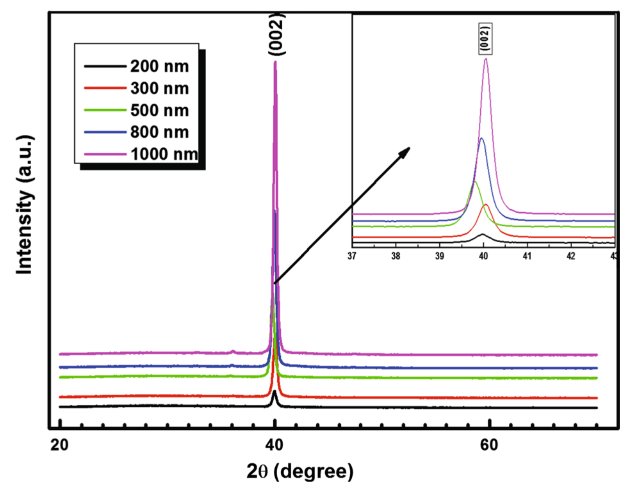

Fig. 3 X-ray diffraction spectrum for ZnO:Ga films with different thickness

On the other hand, the variation in positions of the (002) peak intensity as a function of with the thickness observed in Table 3. As the thickness increases from 200 to 1000 nm, the average crystal size increases from 23 to

Table 2 Variation of the peak intensity (002) depending on the thickness

Deposition time/min	25	40	65	94	160	240
Thickness/nm	200	300	400	500	800	1000
Peak intensity (002)/a.u	2696	9745	6322	13,108	23,539	44,739

Table 3 Variation in the position of the peak (002), grain size, and the distance interticulaire of GZO thin films of different thicknesses

Thickness (nm)	(002) 2θ°	β (deg)	G (nm)	d_{hkl} (Å)	c (Å)	Rms (nm)
200	39.98	0.372	26.43	2.614	5.228	2.75
300	40.04	0.337	29.20	2.613	5.226	3.52
500	39.80	0.340	28.87	2.627	5.254	4.98
800	39.95	0.334	29.40	2.617	5.234	6.81
1000	40.05	0.291	33.76	2.612	5.224	7.12

34 nm, indicating a high thickness improves the crystallinity of the GZO film. The crystal size increased with the increase of thickness, but decreased slightly at 500 nm.

The larger grain size implies the improvement of the crystallinity of the films. From the XRD results, it can be concluded that the film properties are strongly dependent on thickness. The lattice constant c can be calculated by the formula [24]:

$$d_{hkl} = \frac{a}{\sqrt{\frac{4}{3}(h^2 + k^2 + hk) + l^2\frac{c^2}{a^2}}} \quad (2)$$

where a and c are the lattice constants and d_{hkl} is the crystalline plane distance for indices (hkl). According to Eq. (2), the lattice constant c is equal to 2 d_{hkl} for the (002) diffraction peak. The values of d_{hkl} and c are listed in Table 3. All the values of d_{hkl} are larger than that of standard ZnO powder (2.603 Å), indicating that the crystalline plane distances of GZO films are lengthened by imperfections such as lattice strains and interstitial defects. The XRD peak of GZO 3at.% film is moved towards the larger θ values, which leads to a decrease in the lattice parameter c (Table 3). This reduction is directly related to the incorporation of Ga^{3+} ions in substitutional sites Zn^{2+}. Then, the incorporation of the dopant in the ZnO matrix conducts to a network contraction.

Figure 4 shows growth rate of the ZnO:Ga films as a function of the deposition time. When the deposition time is in the range from 25 to 94 min, the growth rate of the films decreases rapidly with increasing the deposition time. As the deposition time is above 100 min, the growth rate decreases slowly and it saturates at 4 nm/min. This is because that at initial stage the film is porous and loose, as time increase, grain sizes becoming larger and the grains become densely packed.

The effect of thickness on the surface state of the deposited layers on glass slides is revealed by atomic force microscopy. AFM images obtained are shown in Fig. 5. It is

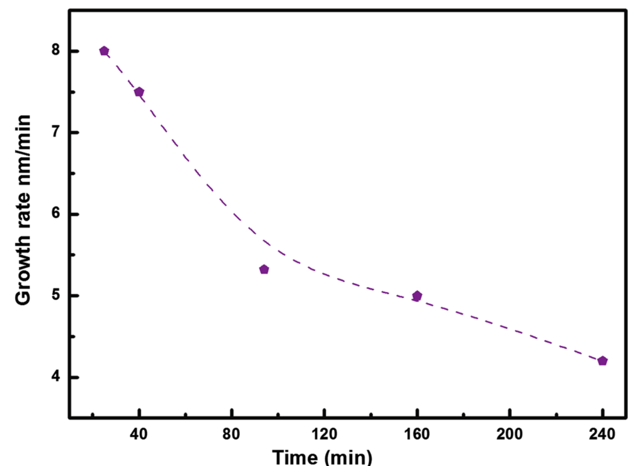

Fig. 4 Growth rate of GZO films as a function of the deposition time

found that the surface condition of the layers is influenced by the increase in thickness. All layers have smooth surfaces. Measurements of roughness are grouped in Table 3. The effect of the thickness of the surface layers deposited on glass slides was investigated. It was found that the surface layers are affected by the increase in thickness. The film crystallite size depends on film thickness. When the deposition begins, there are many nucleation centers on the substrate and small crystallites are produced. With increasing film thickness, the crystallinity of the films is improved and the crystallite sizes become larger. This result is consistent with the XRD observation.

3.3 Electrical properties

The electrical resistivity and Hall Effect measurements have been carried out at room temperature on GZO thin films. The carrier density and mobility of the GZO thin films were estimated from Hall Effect measurements.

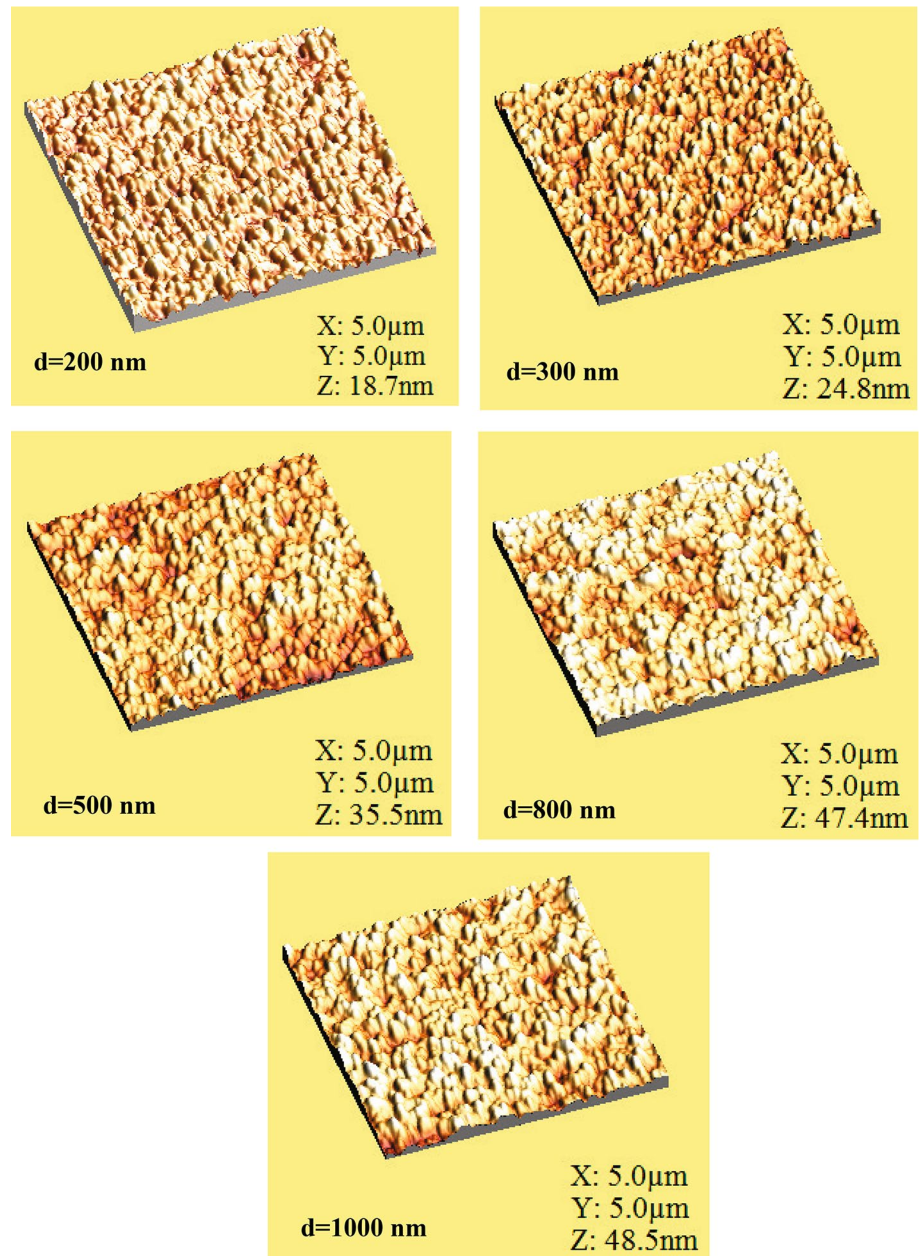

Fig. 5 2D-AFM images ($5 \times 5\ \mu m^2$) of 3at.% Ga-doped ZnO thin films deposited at various thickness

The dependence of the resistivity, Hall mobility and carrier concentration on the thickness of ZnO:Ga films is shown in Fig. 6 and Table 4. It can be seen that, the carrier concentration increases from 0.34 10^{20} to 3 10^{20} cm^{-3} for film thickness than 1000 nm.

The Hall mobility of ZnO:Ga films monotonically increase with increasing the film thickness.

With increasing thickness for the thinner films, the increased mobility is attributed to the improved crystallinity and increased crystallite sizes that weakens inter-crystallite boundary scattering and increases carrier lifetime. The increased mobility and carrier concentration makes the resistivity of the films decrease from 24.3 10^{-3} to 0.810^{-3} (Ω cm) when the film thickness increased from 100 to 1000 nm. The increase in carrier mobility of thin films is attributed to the improved crystallinity and increased crystallite sizes that weaken the inter-crystalline boundary scattering and increases carrier life time [25]. The decrease in the resistivity probably took place due to the increased concentration of dopant gallium atoms in substitutional places of lattice structure under the influence of substrate temperature [15, 26].

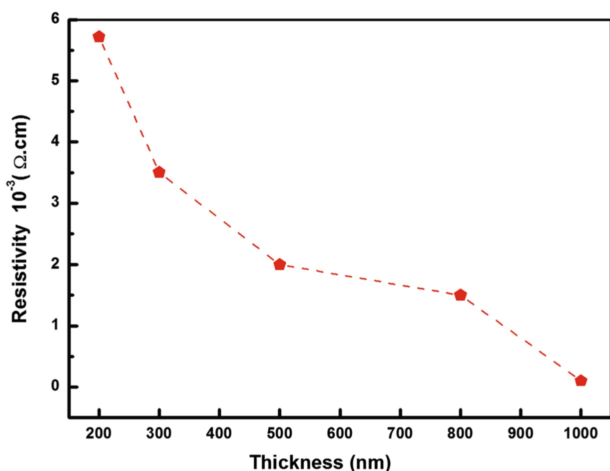

Fig. 6 Variation of resistivities (ρ) as a function with thickness of GZO thin films

Table 4 Electrical properties and band gap of GZO films with different thickness

Thickness (nm)	ρ (Ω cm) 10^{-3}	μ (cm^2/Vs)	n 10^{20} (cm^{-3})	Eg (eV)
200	5.72	8.47	1.28	3.48
300	3.50	9.30	1.92	3.63
500	2.00	14.88	2.10	3.45
800	1.50	16.02	2.60	3.31
1000	0.80	26.04	3.00	3.34

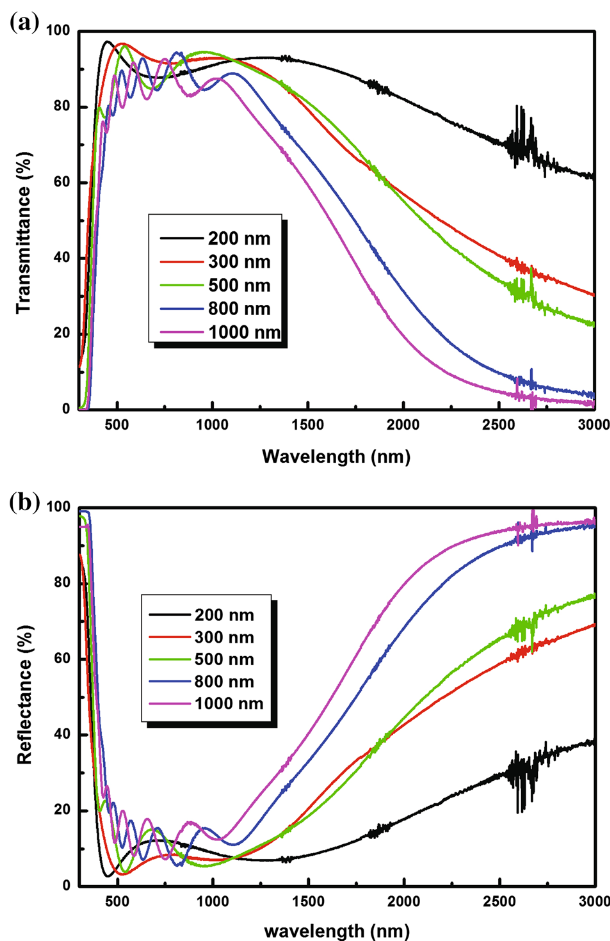

Fig. 7 Transmittance (**a**) and Reflectance (**b**) spectra of GZO thin films of different thicknesses

3.4 Optical studies

The optical transmittance and reflectance of ZnO:Ga 3at.% (GZO 3at.%) films deposited at different thickness, in the spectral range of 200–3000 nm, are shown in Fig. 7 a, b. The observed interference fringes with deep valleys and tall crests indicate that the films have a smooth surface. The steep drop of the transmission for the lower wavelengths at 380 nm, corresponding to absorption in ZnO due to the transition between the valence band and the conduction band. This area is used to determine the energy of the optical gap. According to the theoretical and practical calculations, the ZnO has a direct inter-band transition [27] and for direct allowed transitions between the parabolic bands, the band gap of films was obtained by Tuac's relation [28].

$$\alpha(h\nu) = A(h\nu - E_g)^{1/2} \tag{3}$$

where A is a constant for direct transition, and $h\nu$ is the energy of the incident photon.

The optical absorption coefficient (α) is calculated from the transmittance data, where, the reflection losses are taken into consideration, by [29]:

$$\alpha = \frac{1}{d} Ln \frac{\sqrt{(1-R)^4 + 4T^2R^2} - (1-R)^2}{2TR^2} \tag{4}$$

where d is the thickness of the film and R and T are the reflectance and the transmittance respectively. The optical band gap (E_g) of the films can be obtained by plotting $(\alpha h\nu)^2$ versus $h\nu$ and extrapolating the straight-line portion of plots to the energy axis as shown in Fig. 8 The deduced optical band gaps for films deposited at RT with a thickness 200, 300, 500, 800 and 1000 nm are 3.48, 3.63, 3.45, 3.31 and 3.34 eV, respectively. All the values are larger than that of pure bulk ZnO (3.30 eV). When the thickness is increased, the value of Eg increases rapidly to a thickness of 300 nm and then it decreases. This increase of the gap is caused by the Burstein–Moss effect [30, 31], which is related to the fact the increased concentration of charge carriers block the lowest conduction band states and then transitions can occur only toward higher energy states. The

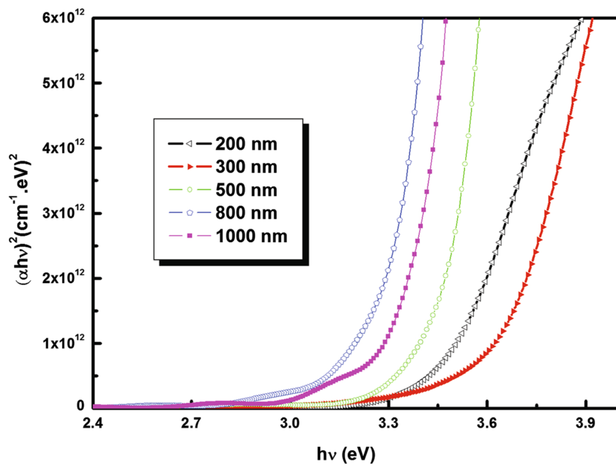

Fig. 8 Square of the absorption coefficient as a function of photon energy for GZO thin films deposited at various thickness

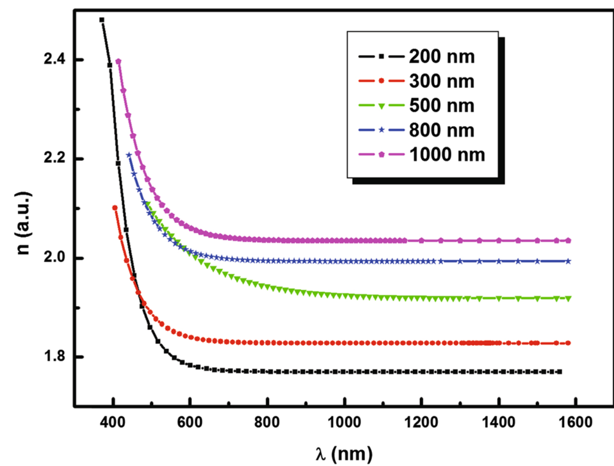

Fig. 9 Variation of refractive index with thickness for GZO films as a function of wavelength

decrease in the energy of the gap can be explained the contradictory phenomena affect the values of the energy gap with the increasing density of donors, mainly in the semiconductor band doped. The band gap of ZnO films at concentrations above the critical concentration holders Mott [32] as the electronic and electro-impurity interaction gives rise to a displacement of the energy bands of valence and conduction, which leads to a reduction of the width of forbidden band. The fundamental absorption edge for ZnO lies in the ultraviolet region and may shift to shorter wave length with increasing carrier density. This shift is due to the filling of states near the bottom of the conduction band.

Zinc oxide is a transparent material whose refractive index in the bulk form is two [33]. In the case of thin films, the refractive index and the absorption coefficient vary depending on the conditions of preparation. The calculated refractive indices at different wavelengths are shown in Fig. 9. The refractive index has a value which varies between 1.80 and 2.50. The improvement in the stoichiometry of ZnO leads to a decrease of the absorption coefficient and an increase in the energy of the band gap. The refractive index of the samples increases with thickness. This increase of the refractive index can be mainly attributed to an increase in carrier concentration in the films ZnO:Ga 3%.

4 Conclusion

ZnO:Ga films were deposited on glass substrate by rf-magnetron sputtering process using aerogel nanopowders prepared by sol–gel technique at low substrate temperature. An investigation of the effects the thickness on the electrical, optical, and structural properties was performed in order to explore the possibility of producing transparent conductive oxide (TCO) films by low-cost process. The crystal structure of the ZnO:Ga films is hexagonal wurtzite and the films are highly oriented along the c-axis perpendicular to the substrates. It has been established that, the effect of the thickness modifies the film growth process and, hence, affects the structure and surface morphology. The deposited layers GZO have a low resistivity, with a minimum value of 10^{-4} Ω cm obtained for the sample deposited at RT with a thickness of 1000 nm. The average transmittances in the visible range for all the films are over 90%. Based on the good conductivity and high transmittance, the GZO films prepared by RF magnetron sputtering can be regarded as a potential transparent electrode.

References

1. H.B. Zeng, W.P. Cai, P.S. Liu, X.X. Xu, H.J. Zhou, C. Klingshrin, H. Kalt, ZnO-based hollow nanoparticles by selective etching: elimination and reconstruction of metal–semiconductor interface, improvement of blue emission and photocatalysis, ACS Nano. **2**, 1661–1670 (2008)
2. C. Klingshirn, ZnO: from basics towards applications, Phys. Status Solid. (b) **244**, 3027–3073 (2007)
3. U. Ozgur, Y.I. Alivov, C. Liu, A. Teke, M.A. Reshchikov, S. Dogan, V. Avrutin, S.-J. Cho, H. Morkoc, A comprehensive review of ZnO materials and devices, J. Appl. Phys. **98**, 041301 (2005)
4. V.S. Khomchenko, T.G. Kryshtab, A.K Savin, Fabrication and properties of ZnO:Cu and ZnO:Ag thin films, Superlattices Microstruct. **42**, 94–98 (2007)
5. H.W. Lee, B.G. Choi, K.B. Shim, Y.J. Oh, Preparation of Ti-doped ZnO transparent conductive thin films by PLD method, J. Ceram. Process. Res. **6**, 52–56 (2005)
6. H. Tang, Z. Ye, L. Zhu, H. He, B. Zhao, M. Zhi, Z. Yang, Synthesis of radial ZnO nanostructures by a simple thermal evaporation method, Phys. E **40**, 507–511 (2008)

7. A.P. Roth, D.F. Williams, Properties of zinc oxide films prepared by the oxidation of diethyl zinc, J. Appl. Phys. **52**, 6685 (1981)
8. L.P. Peng, L. Fang, X.F. Yang, H.B. Ruan, et al., Characteristics of ZnO:In thin films prepared by RF magnetron sputtering, Phys. E Low Dimens. Syst. Nanostruct. **41**, 1819–1823 (2009)
9. P. Nunes, E. Fortunato, R. Martins, Influence of the post-treatment on the properties of ZnO thin films, Thin Solid Films **383**, 277–280 (2001)
10. L.H. Van, M.H. Hong, J. Ding, Structural and magnetic property of Co-doped-ZnO thin films prepared by pulsed laser deposition, J. Alloys Compd. **449**, 207–209 (2008)
11. X.Q. Wei, B.Y. Man, M. Liu, C.S. Xue, H.Z. Zhuang, C. Yang, Blue luminescent centers and microstructural evaluation by XPS and Raman in ZnO thin films annealed in vacuum, N_2 and O_2, Physica B Condens. Matter **388**, 145–152 (2007)
12. A.E. Jimenez-Gonzalez, J.A.S. Urueta, R. Suarez-Parra, Optical and electrical characteristics of aluminum-doped ZnO thin films prepared by sol–gel technique, J. Cryst. Growth **192**, 430–438 (1998)
13. L. Armelao, M. Fabrizio, S. Gialanella, F. Zordan, Sol–gel synthesis and characterisation of ZnO-based nanosystems, Thin Solid Films **394**, 89–95 (2001)
14. G. Aygun, I. Yildiz, Interfacial and structural properties of sputtered HfO{sub 2} layers, J. Appl. Phys. **106**, 014312 (2009)
15. K. Omri, I. Najeh, R. Dhahri, J. El Ghoul, L. El Mir, Effects of temperature on the optical and electrical properties of ZnO nanoparticles synthesized by sol–gel method, Microelectron. Eng. **128**, 53–58 (2014)
16. H. Mahdhi, Z. Ben Ayadi, S. Alaya, J.L. Gauffier, K. Djessas, The effects of dopant concentration and deposition temperature on the structural, optical and electrical properties of Ga-doped ZnO thin films, Superlattices Microstruct. **72**, 60–71 (2014)
17. Z. Ben Ayadi, L. El Mir, K. Djessas, S. Alaya, Electrical and optical properties of aluminum-doped zinc oxide sputtered from an aerogel nanopowder target, Nanotechnology **18**, 445702 (2007)
18. Z. Ben Ayadi, L. El Mir, K. Djessas, S. Alaya, Effect of substrate temperature on the properties of Al-doped ZnO films sputtered from aerogel nanopowders for solar cells applications, Thin Solid Films **519**, 7572–7574 (2011)
19. Y. Chem, D.M. Bagnall, H.K. Koh, K.T. Park, K. Hiraga, Z.Q. Zhu, T. Yao, Plasma assisted molecular beam epitaxy of ZnO on c -plane sapphire: growth and characterization, J. Appl. Phys. **84**, 3912 (1998)
20. B.D. Cullity, *Elements of X-ray Diffraction* (Addison-Wesley, Reading, 1978), p. 102
21. K. Medjnoun, K. Djessas, M.S. Belkaid, S. Grillo, A. Solhy, O. Briot, M. Moret, Characteristics of nanostructured Zn1-xVxO thin films with high vanadium content elaborated by rf-magnetron sputtering, Superlattices Microstruct. **82**, 384–398 (2015)
22. K. Ellmer, R. Cebulla, R. Wendt, Transparent and conducting ZnO:(Al) films deposited by simultaneous RF- and DC-excitation of a magnetron, Thin Solid Films **317**, 413–416 (1998)
23. H. Deng, J.J. Russel, R.N. Lamb, B. Jiang, Microstructure control of ZnO thin films prepared by single source chemical vapor deposition, Thin Solid Films **458**, 43–46 (2004)
24. Min-Chul Jun, Sang-Uk Park, Jung-Hyuk Koh, Comparative studies of Al-doped ZnO and Ga-doped ZnO transparent conducting oxide thin films, Nanoscale Res. Lett. **7**, 639–645 (2012)
25. Xuhu Yu, Jin Ma, FengJi, Yuheng Wang, Chuanfu Cheng, Honglei Ma, Thickness dependence of properties of ZnO:Ga films deposited by rf magnetron sputtering, Appl. Surf. Sci. **245**, 310–315 (2005)
26. G.A. Hirata, J. McKittrick, T. Cheeks, J.M. Siqueiros, J.A. Diaz, O. Contreras, O.A. Lopez, Synthesis and optelectronic characterization of gallium doped zinc oxide transparent electrodes, Thin Solid Films **288**, 29–31 (1996)
27. H. Mahdhi, Z. Ben Ayadi, J.L. Gauffier, K. Djessas, S. Alaya, Effect of sputtering power on the electrical and optical properties of Ca-doped ZnO thin films sputtered from nanopowders compacted target, Opt. Mater. **45**, 97–103 (2015)
28. J. Tauc, Optical properties and electronic structure of amorphous Ge and Si, Mater. Res. Bull. **3**, 37–46 (1968)
29. D.K. Schroder, *Semiconductor Material and Device Characterization*. (Wiley, New York, 1990)
30. E. Burstein, Anomalous optical absorption limit in InSb, Phys. Rev. **93**, 632–633 (1954)
31. T.S. Moss, The Interpretation of the Properties of Indium Antimonide, Proc. Phys. Soc. B **67**, 775–782 (1954)
32. M.A. Lucio-Lopez et al., Thickness dependence of ZnO:In thin films doped with different indium compounds and deposited by chemical spray, Sol. Energy Mater. Sol. Cells **90**, 2362–2376 (2006)
33. R.C. Weast, *Handbook of Chemistry and Physics*, 56th edn. (CRC Press, Cleveland, 1975), pp. B–204